Fluorescent oxygen sensitive microbead incorporation for measuring oxygen tension in cell aggregates

Dennis Lambrechts[a,c], Maarten Roeffaers[b], Greet Kerckhofs[a,c], Scott J. Roberts[c], Johan Hofkens[d], Tom Van de Putte[e], Hans Van Oosterwyck[c,f], Jan Schrooten[a,c,*]

[a] Department of Metallurgy and Materials Engineering, KU Leuven, Kasteelpark Arenberg 44 – box 2450, 3001 Leuven, Belgium.

[b] Center for Surface Chemistry and Catalysis, KU Leuven, Kasteelpark Arenberg 23, 3001 Leuven, Belgium.

[c] Prometheus, Division of Skeletal Tissue Engineering Leuven, KU Leuven, Herestraat 49 – box 813, 3000 Leuven, Belgium.

[d] Molecular Imaging and Photonics, KU Leuven, Celestijnenlaan 200F, 3001 Leuven, Belgium.

[e] TiGenix NV, Haasrode Researchpark 1724, Romeinse straat 12 box 2, 3001 Leuven, Belgium.

[f] Biomechanics Section, KU Leuven, Celestijnenlaan 300C – box 2419, 3001 Leuven, Belgium.

[*] To whom correspondence may be addressed.

E-mail: Jan.Schrooten@mtm.kuleuven.be

Jan Schrooten, Kasteelpark Arenberg 44 – box 2450, 3001, Leuven, Belgium

Abstract

Molecular oxygen is a main regulator of various cell functions. Imaging methods designed as screening tools for fast, *in situ*, 3D and non-interfering measurement of oxygen tension in the cellular microenvironment would serve great purpose in identifying and monitoring this vital and pivotal signalling molecule. We describe the use of dual luminophore oxygen sensitive microbeads to measure absolute oxygen concentrations in cellular aggregates. Stable microbead integration, a prerequisite for their practical application, was ensured by a site-specific delivery method that is based on the interactions between streptavidin and biotin. The spatial stability introduced by this method allowed for long term measurements of oxygen tension without interfering with the cell aggregation process. By making multiple calibration experiments we further demonstrated the potential of these sensors to measure local oxygen tension in optically dense cellular environments.

Introduction

Oxygen is an important regulator of cell behaviour, both at a cell/tissue level and a molecular level. Based on its relatively low solubility in culture medium, oxygen gets easily depleted in static 3D culture systems[1]. This becomes most apparent in culture systems which have tight cell packing, such as cellular aggregates[2], or within a dense biomaterial carrier (for example, fibrin) [3]. Critical gradients will arise in these systems resulting from the interplay between diffusion (driven by differences in local oxygen concentration) and cellular consumption[4].

As a key component for cellular energy generation through oxidative phosphorylation, local oxygen depletion impairs cell survival when sustained over critical periods of time[5], even independent of local nutrient concentrations[6]. Most cells however are able to survive and recover from hypoxic conditions. This is accomplished by transcription factor-regulated (such as Hypoxia Inducible Factor (HIF) [7, 8]) mechanisms, that among others control energy metabolism and the cell cycle and that result in the ability to decrease oxygen utilization rate under low oxygen tension (i.e. oxygen conformity) [9, 10].

Oxygen levels also serve as a developmentally important stimulus. These oxygen regulation processes have been studied in skeletal development[11]. Endochondral ossification starts with the formation of precartilaginous condensations which originate from small cellular aggregates that expand through concerted cell activities including cell proliferation, migration, adhesion and differentiation[12]. *In vitro* studies have indicated that high cellularity and the

avascular nature are important prerequisites for cartilage cell differentiation[13, 14], creating locally low oxygen tension and nutrient concentration, which is favourable for subsequent cartilage differentiation[15].

Investigating and understanding the mechanisms which underlie the process of chondrogenesis can be achieved *in vitro* using appropriately designed setups. Proper *in vitro* recapitulation of micro-environmental biophysical signals such as oxygen tension and cell-cell interactions is thereby mandatory[16]. An excellent model that is able to mimic condensation and chondrogenic differentiation *in vitro* is represented by cell aggregate cultures[17]. This culture system provides an appropriate 3D environment for synthesis, and deposition of cartilage matrix proteins, and is amenable to morphological, proteomic or transcriptional analysis[17]. Cell aggregates have been proposed as elementary building blocks for creating cell-based products using a modular design approach[18-20]. Though the influence of oxygen on cell fate is widely acknowledged, tools for non-invasively monitoring local oxygen concentrations in such dense cell environments are still limited or have major shortcomings.

Measurement of oxygen tension by the use of oxygen sensitive microfibers or micro-electrodes is complicated by the very small dimensions of cell aggregates. Furthermore such devices would strongly interfere with internal aggregate mass transport by inducing cell damage or creating 'leaky paths' at the probed positions. This issue is circumvented by the use of non-invasive probes[21, 22]. An example of this are perfluorocarbon (PFC) microdroplets, such as hexafluorobenzene, which rely on the paramagnetic properties of molecular

4

oxygen to alter ^{19}F nuclear magnetic resonance (NMR) relaxation times of the PFCs in direct proportion to the dissolved oxygen concentration[23]. These microdroplets diffuse and accumulate into interstitial spaces where they report on local oxygen tensions[24]. NMR measurements have however a rather low spatial resolution which limits their use for the small aggregate dimensions. The application of paramagnetic probes, such as trityl radicals, combined with electron paramagnetic resonance (EPR) is a very promising approach that provides reasonable resolution images (~10-30 μm) within acceptable acquisition times (minutes)[25]. Dual luminophore oxygen-sensing beads (OSBs) also offer great possibilities for measuring oxygen tension in a fast and non-interfering manner and have been developed for measuring local oxygen tension in (poly(ethylene glycol)dimethylacrylate) hydrogel carriers[26, 27]. As the absence of controlled, site-specific delivery methods for these probes have prevented so far their practical application to cellular systems, we developed a non-invasive method for spatially controlled microbead incorporation into dense cell aggregate environments and assessed its feasibility to measure local oxygen tension.

Materials and Methods

Cell culture

ATDC5 cells (Riken Cell Bank, Tsukuba, Japan), a murine chondrogenic cell line,[28] were grown in maintenance medium consisting of a 1:1 mixture of Dulbecco's modified Eagle's medium (DMEM) and Ham's F-12 medium (Invitrogen) supplemented with 5% foetal bovine serum (Gibco), antibiotic-

antimycotic (A/A) solution (100 units/ml penicillin, 100 µg/ml streptomycin, and 0.25 µg/ml amphoterecin B; Invitrogen), 10 µg/ml human transferrin (Roche Molecular Biochemicals), and 3×10 M sodium selenite (Sigma). Medium was refreshed every 2 to 3 days and cells passaged when sub-confluent.

Production of fluorescent microbeads

OSBs were synthesized according to a protocol, adapted from Acosta *et al.*[26] and is composed of three steps (first two steps identical to Acosta *et al.*).

Production of Ru(Ph$_2$phen$_3$)Cl$_2$-bound silica gel beads – The core material of the OSB consists of silica gel (Davisil 710, 236756, Sigma) and has a diameter of 9.5 to 11 µm. Silica gel beads contain hydroxyl groups at their surfaces, making them very polar. An initial amount of 2 g silica gel was brought into solution with a 40 ml aqueous NaOH (0.01 N) solution and stirred at high speed (1000 rpm, 3.5 cm stir bar) for 30 min. Fluorescent molecules used for oxygen measurement are the oxygen sensitive Tris (4,7-diphenyl-1,10-phenanthroline) ruthenium (II) dichloride (76886, Sigma) and an oxygen insensitive reference fluorophore, Nile blue chloride (222550, Sigma). Two 10 ml solutions were prepared containing these molecules in concentrations of 0.5 mM. These solutions were poured into the silica gel solution and stirred (30 min, 1000 rpm). Afterwards the beads were centrifuged (1900xg, 10 min) and washed three times in deionized water (30 ml) and once in ethanol (30 ml). Supernatant was removed and the beads were dried overnight at 70°C.

Encapsulation of silica gel beads – In order to avoid problems with toxicity of the Ru(Ph$_2$phen$_3$)Cl$_2$ luminophore, beads were encapsulated in a

poly(dimethylsiloxane) (PDMS) layer. To this end 0.2 g Ru(Ph$_2$phen$_3$)Cl$_2$-bound silica gel beads were mixed with 1 g PDMS pre-polymer (Sigma), 0.1 g curing agent (Sylgard 184 elastomer kit, part B, Dow Corning), and 700 µl hexane (Sigma). This solution was gently vortexed with a pipette tip (~1-3 min) and rested for ~30 min. It was then transferred to a heated (70°C) sodium dodecyl sulfate (SDS, 2w/v%, 300 ml) solution and stirred (1200 rpm, 3.5 cm stir bar) for ~7-8 hours. The combined use of a vortexer and SDS solution prevented the emulsified beads from clustering, while heating the solution resulted in curing and solidification of the PDMS polymer. Suspended beads were collected by centrifugation (2500xg, 20 min) and washed three times in PBS solution (30 ml).

Coating of bead surfaces with streptavidin molecules – The bead solution was autoclaved and supernatant removed after centrifugation (1900xg, 10 min). Beads (~1x10^7) were incubated at low temperature (4°C) in 1 ml maintenance medium (DMEM:F12, 5% FBS, 1% A/A, 3x10^{-8} M sodium selenite, 10 µg/ml human transferrin) supplemented with 50 µl of an Alexa Fluor 488 labelled streptavidin solution (2 mg/ml) for ~24 hours. Produced OSBs were centrifuged (1900xg, 10 min) and resuspended in maintenance medium.

OSB fluorescence microspectroscopy

Fluorescent spectra of the OSBs were measured on a Fluoview 1000 microscope (Olympus). Samples were excited with a 488 nm laser for Alexa Fluor 488 and Ru(Ph$_2$phen$_3$)Cl$_2$ detection and with a 635 nm laser for detection of the Nile Blue chloride. A lambda series was subsequently recorded using the FV10-ASW software package (Olympus). Fluorescence emission was detected with a step

size of 2 nm and a bandwidth of 4 nm, which was measured in a wavelength range of 500 nm to 750 nm. Both spectra were normalized and overlaid for visual representation.

OSB calibration

Oxygen sensitive microbeads were exposed to different oxygen tensions by perfusing Argon gas in an air-tight workhead (Solent Scientific). A glass bottom dish (Ø 35 mm) was positioned centrally into the workhead in which OSBs were either contained in a PBS solution, PBS solution with 200 µm thick agarose (2%) spacer or incorporated in an ATDC5 cell aggregate suspended in maintenance medium. Prior to image acquisition, we treated the cell aggregates with a NaN_3 (5 mM) solution to avoid any influence of the cellular oxygen uptake on the measurement read-outs. Microbeads were visualized on a confocal laser scanning microscope (Fluoview 1000, Olympus) equipped with a UPLSAPO 20x air objective (NA: 0.75). Excitation of the beads was performed with a 488 nm Ar laser for detection of the ruthenium complex (2.5 µW in liquid configuration, 25 µW with agarose spacer and 50 µW in aggregate configuration, which is the power measured after the objective) and for detection of the Alexa Fluor 488 (10 µW in aggregate configuration). For visualization of the Nile Blue chloride 635 nm HeNe laser was used (20 µW in liquid configuration, 22 µW with agarose spacer and 40 µW in aggregate configuration). Fluorescence emission was detected with a DM375-405/488/559/635 primary beam splitter in combination with a BA575-620 emission filter for detection of the ruthenium complex and a BA655-755 emission filter for detection of the Nile Blue. Reference oxygen

measurements were performed in a separate dish using a luminescent needle probe (neoFox, Ocean Optics). Images were taken after stable oxygen tension measurements of at least 10 min for OSBs in PBS solution or 30 min for OSBs incorporated in a cell aggregate. All experiments were performed at 37°C incubation temperature.

A particle-based calibration was performed in ImageJ by defining regions of interest around individual beads (each image contained at least 15 beads). These regions were defined based on binary images of a single reference fluorophore. Mean intensities were subsequently measured for each fluorescent dye contained on the bead. These values were finally inserted into the Stern-Volmer equation,

$$\frac{I_{R,0}}{I_R} - 1 = K_D\left[O_2\right]$$

where $I_{R,0}$ and I_R are the fluorescence intensities of the oxygen sensitive luminophore Ru(Ph$_2$phen$_3$)Cl$_2$ in absence or presence of molecular oxygen respectively, normalized to the reference fluorophore intensity (Nile Blue or Alexa Fluor 488); K_D is the Stern-Volmer quenching constant; and [O_2] is the reference oxygen tension at which an intensity value of I_R was measured.

Biotinylation of cell surfaces

To functionalize ATDC5 cell surfaces for OSB binding, we followed a protocol previously described by De Bank *et al.*[29] Cells were grown to ~60 to 80% confluency, trypsinized and counted with a haemocytometer. Expression of aldehyde groups on the cell surfaces resulted from subsequent incubation with 5

ml cold (4°C) sodium periodate ($NaIO_4$) solution in a dark environment for ~5-10 min. This solution was diluted with PBS afterwards and washed in 5 ml biotinylation buffer (PBS, 0.1% FBS, pH 6.5, RT). Biotin adhesion was allowed by incubation of the cells with 5 ml biotin hydrazide solution (5 mM in biotinylation buffer) for ~30 min at RT. The cell suspension was finally washed in 5 ml cold streptavidin buffer (PBS, 0.1% FBS, pH7.0). This procedure is illustrated in **Figure S1**.

Production and cultivation of cell aggregates

Following biotinylation of the cell surfaces, ATDC5 cells were resuspended in maintenance medium (37.5×10^5 cells/ml). This solution contained the OSBs in a concentration of 0.2% (number of beads per number of cells). Initial addition of the beads was required for a homogeneous distribution in the developing aggregate. Next, 40 µl of the cell-OSB solution was poured into the wells of a V-bottom polypropylene 96-well plate and cultivated for 24 hours to achieve stable aggregate formation. After this period the medium was replenished to a final volume of 200 µl, which was refreshed every 2 to 3 days.

Conjugation and stability assay of avidin biotin binding

ATDC5 cells, untreated (control group) or functionalized with biotin molecules (biotin group), were plated as confluent monolayers (100,000 cells/cm^2) in wells of an 8-chamber slide (Lab-Tek®, Nunc). Cell attachment was allowed for 3 hours, after which the wells were rinsed with PBS to remove any non-adherent cells. Medium (200 µl) containing the OSBs in a concentration of 5% was added to the wells. Analyses were performed at defined time points by brightfield

imaging of the adherent cells and fluorescence detection of the cell-conjugated OSBs. Four different wells were visualized at random locations for each time point and processed in ImageJ for quantification of the total amount of cells and beads. Beads were regarded as cell-conjugated when their contours were in close vicinity or had a significantly overlapping region. At the onset of each analysis, wells were rinsed once again to discard the non-conjugated beads.

DNA quantification

DNA content was evaluated according to a protocol described by Grayson *et al.*[30] Briefly, cell aggregates were washed in PBS, transferred to 1 ml of digestion buffer (10 mM Tris, 1mM EDTA, and 0.1% Triton X-100) with 0.1 mg/ml proteinase K in centrifugation tubes, and incubated overnight at 56°C. Supernatant was collected after removal of debris by centrifugation (13,000 rpm, 1 min) and measured with a Qubit system (Invitrogen).

Cell metabolic activity

Metabolic activity of the cell aggregates was measured using the alamarBlue® reagent (Invitrogen), according to the manufacturer's instructions. The reagent was added as 10% of the medium volume, followed by a 3 hour incubation period at 37°C. Resulting fluorescence of 100 µl medium samples were measured in duplicate on a plate reader (Perkin Elmer) and corrected for background fluorescence.

Cell viability assay

We analysed cell viability using the LIVE/DEAD viability/cytotoxicity kit (Invitrogen). Cell aggregates were rinsed with PBS solution, covered with

LIVE/DEAD staining solution containing 2 μM calcein AM and 4 μM ethidium homodimer-1 in PBS, and incubated for 30 min in the dark. The dye solution was discarded afterwards and background due to residual stain was washed away with PBS. Aggregates were transferred to a glass bottom dish (MatTek) and visualized with a confocal laser scanning microscope (CLSM 510 META NLO, Zeiss).

Histological analysis

At defined time points during culture, cell aggregates were analysed by histology. Aggregates were washed with PBS, fixed overnight in 4% formaldehyde, and suspended in 2% agarose gels. Suspensions were subsequently embedded in paraffin and cut at 5 μm thick cross-sections which were then processed according to the specific histological staining.

Apoptosis assay

Apoptosis inside cell aggregates was assayed by TUNEL staining. This staining was performed according to the manufacturer's instructions (In situ cell death detection kit, Roche).

Pimonidazole staining

Hypoxic regions were identified after 3 hours incubation of the ATDC5 cell aggregate in a 0.2 μM pimonidazole hydrochloride solution. To visualize the formation of pimonidazole adducts, cell aggregate paraffin sections were immunostained with Hypoxyprobe-1-Mab1 (Hypoxyprobe kit, Chemicon) following the manufacturer's instructions.

Results

OSBs incorporating an oxygen sensitive luminophore ($Ru(Ph_2phen_3)Cl_2$) and two reference fluorophores (Nile Blue chloride and Alexa Fluor 488) were produced and characterized (**Figure 1A**). The OSBs showed in their fluorescence spectra peak values near 505 nm (Alexa Fluor 488) and 610 nm (ruthenium complex) for excitation with a 488 nm laser, and near 655 nm (Nile Blue) for excitation with a 635 nm laser (**Figure 1B**), which indicates the incorporation of all fluorescent molecules by the bead. The selected ruthenium complex has a long unquenched lifetime after excitation[31]. Presence of molecular oxygen quenches the fluorescent signal in a diffusion-controlled manner (i.e. collisional quenching) and is described by the Stern-Volmer theory[31]. Fluorescence intensity is therefore inversely proportional to the quencher concentration. Microbeads were calibrated by measurement of fluorescence intensity values at controlled environmental oxygen levels, ranging from 0% to 21% O_2. However, the fluorescent signal passing through an optically dense environment can be absorbed and scattered, both influencing the measured intensity. To compensate for this loss, the obtained values were normalized to the intensity of a stable, oxygen-insensitive reference fluorophore. This resulted in a linear Stern-Volmer plot for OSBs suspended in a transparent liquid (**Figure 1E**), which suggests an equal accessibility of all $Ru(Ph_2phen_3)Cl_2$ molecules to the oxygen quencher. In this configuration, OSBs were characterized by a quenching constant K_{Dm} of 0.0076 ± 0.0019 $\mu mol^{-1} \cdot L$ (average ± standard deviation). As expected, introduction of an

agarose spacer of approximately 200 micron thickness between the microscope objective and OSBs (**Figure 1E**) did not change the Stern-Volmer relation significantly. In this case the quenching behavior was characterized by a quenching constant K_{Da} of 0.0079 ± 0.0020 µmol^{-1}·L.

To test the OSBs in combination with a cell system, three-dimensional (3D) cell aggregate cultures were made of ATDC5 cells, a murine chondrogenic cell line[28]. Because of the disparity in density between OSBs and cells, forced conjugation was anticipated to assure robust integration and uniform distribution of the fluorescent beads into the dense cell aggregate environment. A method based on the interaction between streptavidin and biotin (SB) was chosen [29, 32]. Taking advantage of the strong adsorption properties of streptavidin to a poly(dimethylsiloxane) (PDMS) layer[33], bead surfaces were coated uniformly with streptavidin molecules (**Figure 2**). Cell surfaces were prepared for interaction with the coated microbeads by periodate treatment followed by biotin conjugation[29]. This approach resulted in a complete inclusion of the fluorescent beads by conjugated cells during the initial phase of aggregation (**Figure S1**) and homogeneous distribution of OSBs in the aggregate (**Figure 1D**). As a reduction in conjugated amount of biotin molecules to ~25% after a 24 hour period has been reported previously in literature,[29] we addressed the temporal change in interaction ability of biotin-coated cells with the streptavidin-coated OSBs. In a 2-dimensional (2D) conjugation stability assay it was shown that cells maintain their ability to interact with the OSBs, even after a 24 hour incubation period (**Figure 3**).

Next, the non-interfering nature of bead integration into the cell aggregate was investigated. Aggregates from control groups (no OSBs and no SB treatment, group I) were compared with aggregates resulting from SB treated cells (group II) and from SB treated cells with OSB addition (group III). Functional behaviour of these three groups was quantified in terms of DNA content, metabolic activity, cell viability, aggregate morphology, and oxygen mass transport at discrete time points during a one week *in vitro* cultivation process.

DNA content for all groups rapidly dropped over time reaching almost half of the initial seeded cell amount after 7 days (**Figure 4A**). This observation is in line with previous studies reporting on the cultivation of dedifferentiated or undifferentiated chondrocyte pellets under saturated oxygen conditions (21% O_2) [34, 35]. In these studies chondrogenic (re-)differentiation, either by growth factor induction (TGF-β and insulin) or by changing oxygen tension to lower values (~5% O_2), resulted in a stabilization of DNA content. A similar decreasing trend in function of time, though less pronounced, was seen in the metabolic activity of cell aggregates (**Figure 4B**). No statistically significant differences (student t-test, $p < 0.05$) could be found between the aggregate groups, neither in DNA content nor in metabolic activity. Aggregate diameter gradually decreased with longer cultivation time, which was consistent with the measured drop in DNA content. Aggregate size (**Figure 4C**) and morphology, as assessed by Hematoxylin & Eosin (H&E) staining and fluorescent confocal imaging (**Figure 4D**), were however comparable between the different groups at a particular time point. All aggregates of all different experimental groups were characterized by a high

15

fluorescent calcein-AM signal at all time points analysed (**Figure S2**), indicative for the presence of living cells, and all contained a region of apoptotic cells, that manifested from peripheral to central regions of the pellet (**Figure 4E**). Finally the transport of molecular oxygen inside the cell aggregate was assessed by detection of hypoxic regions using a pimonidazole staining. Similar patterns between the different conditions were observed (**Figure 5**). Stable aggregate formation, similar aggregate size and morphology as well as similar cell behaviour indicated that SB-mediated OSB interaction did not interfere with normal cell to cell contacts that take place during the cell aggregation phase.

Cell aggregate embedded OSBs were visualized at different oxygen tensions. A uniform distribution of oxygen tension inside the aggregate was obtained after a 12 hour treatment period of the aggregates with NaN_3, which is an inhibitor of the aerobic cellular metabolism (cytochrome-c oxidase activity). Though ATDC5 cell autofluorescence overruled the Nile Blue fluorescence signal, the used calibration procedure still gave rise to a linear Stern-Volmer relation using the Alexa Fluor 488 signal as a reference (**Figure 1F**). A quenching constant K_{Dc} of 0.0091 ± 0.0035 $\mu mol^{-1} \cdot L$ was obtained.

Discussion

Many aspects of normal cell function, ranging from basic cell respiration to integrin-mediated adhesion behaviour[1], depend on the availability of molecular oxygen. Given the important biophysical functionality, *in vitro* model systems would greatly benefit from *in situ* read-outs on local oxygen tension. These

systems could for example reveal nutrient delivery problems during aggregate production in the context of tissue-engineering approaches[36, 37] or help identifying interesting biological activity of drugs investigated in cell array cultures.[38] Fluorescent microbeads stably incorporated into a cell aggregate have great potential to provide these crucial data by making ratiometric measurements of an oxygen-sensitive luminophore with an oxygen-insensitive reference fluorophore. The major advantage of such dual luminophore oxygen sensitive microbeads as a screening tool mainly comes from the potential to make fast measurements of oxygen tension in the same microenvironment over long periods of time. As a first step, we have described the production of such beads, their calibration and a method for non-interfering, spatially controlled incorporation and uniform distribution into cell aggregates.

As a carrier material for the fluorescent probes, silica beads were used. This silica material possesses a pH-adjustable cation exchange capacity, which allowed for ionic binding with the $Ru(Ph_2phen_3)Cl_2$ luminophore[39], and high polarity, which gave rise to an increased quenching rate[40]. OSBs calibrated at different oxygen tensions showed linearity in the Stern-Volmer relationship for beads suspended in a liquid monolayer or in the presence of a turbid agarose spacer. Embedding microbeads in the cell aggregate resulted in loss of the Nile Blue signal due to high autofluorescence of the ATDC5 cells when excited at 635 nm which strongly overlaps with the Nile Blue signal. The presence of a second reference fluorophore that we introduced in this study however resolved this problem, giving rise to the linear calibration curve (**Figure 1F**).

Application of the streptavidin-biotin interaction has been previously described for the assembly of multicellular aggregates[29, 41, 42]. Here, we further broaden the application range and report the efficacy of this conjugation method for integrating fluorescent probes into cartilaginous cell aggregates. The integration stability and non-interfering behaviour of OSB-containing aggregates was shown through various assays at discrete time points during cultivation.

Viability of the aggregated cells was comparable between the groups. Interestingly, a region of apoptotic cells was reproducibly detected and apparently correlated with the distribution of oxygen depleted regions as observed from the pimonidazole staining. These hypoxic regions could possibly originate from the fusing of aggregate edges after the initial aggregation phase (**Figure S3**). Aggregate formation will thereby embed the outer layer of the aggregate which consist of several layers of elongated cells into deeper zones, resulting in a change of their oxygen accessibility from relatively high (as diffused in the culture medium) to nearly hypoxic conditions inside the aggregate. As this type of cells may not be adapted to such adverse environment, cell death would plausibly occur. Robust and efficient incorporation of the microbeads into the cell aggregate was dependent on the strong noncovalent interaction between streptavidin and biotin (**Figure 1C,D**). As cells normally express biotin (vitamin H) at very low concentrations[43, 44], and hence have a low possibility for microbead interaction, we needed to increase the total amount of biotin molecules presented on the cell surfaces. The strategy applied here was to

precede cell surface biotinylation with a periodate treatment. This procedure has been shown to yield a 1,000-fold increase in total biotin expression[45].

The need for a high initial amount of biotin molecules stems from observations in literature reporting a strong reduction in biotin presence on the cell surfaces already after 24 hours[29]. This reduction would impair good incorporation of the microbeads in the cell aggregate, as cell condensation and associated bead intercalation occurs within this period. Conjugation stability assays confirmed microbead interaction abilities with the biotinylated cells remained even after an incubation period of 24 hours (**Figure 3**).

The presented method is not limited to controlled delivery and encapsulation of microbeads in dense cell environments. With recent reports on more stable streptavidin variants, such as traptavidin[46], this method could also be explored for long term monitoring of oxygen tension in macro- or microporous scaffolds or the small medium volumes applied in lab-on-a-chip systems.

Conclusions

In this study we described the application of fluorescent oxygen sensitive microbeads (OSBs) within three dimensional cell aggregates for highly localized, quantitative measurements of oxygen tension. Successful integration of the fluorescent microbeads into cell aggregates was obtained by a binding method that relied on the interaction between biotinylated cell surfaces and streptavidin coated microbeads. We showed the non-interfering behaviour of OSB-containing aggregates through various assays at discrete time points during static

19

cultivation. Calibration of OSBs at different oxygen tensions showed linearity in the Stern-Volmer relationship for beads suspended in a liquid, in the presence of an agarose spacer, or when embedded in a cell aggregate. By coupling local and quantitative measurements of oxygen tensions with specific cell behaviour, the presented method for integration of OSBs into cellular aggregates can significantly improve understanding of the role of oxygen in cellular environments.

References

[1] Griffith LG, Swartz MA. Capturing complex 3D tissue physiology in vitro. Nat Rev Mol Cell Bio. 2006;7:211-24.

[2] Glicklis R, Merchuk JC, Cohen S. Modeling mass transfer in hepatocyte spheroids via cell viability, spheroid size, and hepatocellular functions. Biotechnol Bioeng. 2004;86:672-80.

[3] Demol J, Lambrechts D, Geris L, Schrooten J, Van Oosterwyck H. Towards a quantitative understanding of oxygen tension and cell density evolution in fibrin hydrogels. Biomaterials. 2011;32:107-18.

[4] Beard DA, Qian H. Chemical Biophysics: Quantitative Analysis of Cellular Systems. New York: Cambridge University Press; 2008.

[5] Radisic M, Malda J, Epping E, Geng WL, Langer R, Vunjak-Novakovic G. Oxygen gradients correlate with cell density and cell viability in engineered cardiac tissue. Biotechnol Bioeng. 2006;93:332-43.

[6] Derda R, Laromaine A, Mammoto A, Tang SK, Mammoto T, Ingber DE, et al. Paper-supported 3D cell culture for tissue-based bioassays. Proc Natl Acad Sci USA. 2009;106:18457-62.

[7] Kim JW, Tchernyshyov I, Semenza GL, Dang CV. HIF-1-mediated expression of pyruvate dehydrogenase kinase: A metabolic switch required for cellular adaptation to hypoxia. Cell Metab. 2006;3:177-85.

[8] Lahiri S, Roy A, Baby SM, Hoshi T, Semenza GL, Prabhakar NR. Oxygen sensing in the body. Prog Biophys Mol Bio. 2006;91:249-86.

[9] Hochachka PW, Lutz PL. Mechanism, origin, and evolution of anoxia tolerance in animals. Comp Biochem Phys B. 2001;130:435-59.

[10] Hochachka PW, Buck LT, Doll CJ, Land SC. Unifying theory of hypoxia tolerance: Molecular metabolic defense and rescue mechanisms for surviving oxygen lack. P Natl Acad Sci USA. 1996;93:9493-8.

[11] Karsenty G, Wagner EF. Reaching a genetic and molecular understanding of skeletal development. Developmental Cell. 2002;2:389-406.

[12] Hall BK, Miyake T. Divide, accumulate, differentiate: Cell condensation in skeletal development revisited. Int J Dev Biol. 1995;39:881-93.

[13] Archer CW, Rooney P, Wolpert L. Cell-Shape and Cartilage Differentiation of Early Chick Limb Bud Cells in Culture. Cell Differ Dev. 1982;11:245-51.

[14] Abbott J, Holtzer H. Loss of Phenotypic Traits by Differentiated Cells .V. Effect of 5-Bromodeoxyuridine on Cloned Chondrocytes. P Natl Acad Sci USA. 1968;59:1144-&.

[15] Caplan AI, Koutroup.S. Control of Muscle and Cartilage Development in Chick Limb - Role of Differential Vascularization. J Embryol Exp Morph. 1973;29:571-83.

[16] Lambrechts D, Schrooten J, Van de Putte T, Van Oosterwyck H. Computational Modeling of Mass Transport and Its Relation to Cell Behavior in Tissue Engineering Constructs. In: Geris L, editor. Studies in Mechanobiology, Tissue Engineering and Biomaterials. Berlin Heidelberg: Springer-Verlag 2012.

[17] Welter JF, Solchaga LA, Penick KJ. Simplification of aggregate culture of human mesenchymal stem cells as a chondrogenic screening assay. Biotechniques. 2007;42:732-+.

[18] Lenas P, Moos M, Luyten FP. Developmental engineering: a new paradigm for the design and manufacturing of cell-based products. Part I: from three-dimensional cell growth to biomimetics of in vivo development. Tissue Eng Part B Rev. 2009;15:381-94.

[19] Barbero A, Scotti C, Tonnarelli B, Papadimitropoulos A, Scherberich A, Schaeren S, et al. Recapitulation of endochondral bone formation using human adult mesenchymal stem cells as a paradigm for developmental engineering. P Natl Acad Sci USA. 2010;107:7251-6.

[20] Wolf F, Candrian C, Wendt D, Farhadi J, Heberer M, Martin I, et al. Cartilage tissue engineering using pre-aggregated human articular chondrocytes. Eur Cell Mater. 2008;16:92-9.

[21] Gallez B, Baudelet C, Jordan BF. Assessment of tumor oxygenation by electron paramagnetic resonance: principles and applications. Nmr Biomed. 2004;17:240-62.

[22] Vikram DS, Zweier JL, Kuppusamy P. Methods for noninvasive imaging of tissue hypoxia. Antioxid Redox Sign. 2007;9:1745-56.

[23] Grucker D. Oxymetry by magnetic resonance: applications to animal biology and medicine. Prog Nucl Mag Res Sp. 2000;36:241-70.

[24] Ratner AV, Muller HH, Simpson BB, Johnson DE, Hurd R, Young SW. Detection of Tumors with F-19 Magnetic-Resonance-Imaging. Invest Radiol. 1987;22:S10-S.

[25] Halevy R, Tormyshev V, Blank A. Microimaging of oxygen concentration near live photosynthetic cells by electron spin resonance. Biophys J. 2010;99:971-8.

[26] Acosta MA, Ymele-Leki P, Kostov YV, Leach JB. Fluorescent microparticles for sensing cell microenvironment oxygen levels within 3D scaffolds. Biomaterials. 2009;30:3068-74.

[27] Acosta MA, Velasquez M, Williams K, Ross JM, Leach JB. Fluorescent silica particles for monitoring oxygen levels in three-dimensional heterogeneous cellular structures. Biotechnol Bioeng. 2012.

[28] Tare RS, Howard D, Pound JC, Roach HI, Oreffo ROC. Development of tissue engineering strategies for cartilage generation: Micromass and three dimensional cultures using human chondrocytes and an immortalized cell line. J Bone Miner Res. 2005;20:1300-.

[29] De Bank PA, Kellam B, Kendall DA, Shakesheff KM. Surface engineering of living myoblasts via selective periodate oxidation. Biotechnol Bioeng. 2003;81:800-8.

[30] Grayson WL, Frohlich M, Yeager K, Bhumiratana S, Chan ME, Cannizzaro C, et al. Engineering anatomically shaped human bone grafts. Proc Natl Acad Sci U S A. 2010;107:3299-304.

[31] Lakowicz JR. Principles of Fluorescence Spectroscopy. 3 ed. Baltimore: Springer; 2006.

[32] Gothard D, Roberts SJ, Shakesheff KM, Buttery LD. Engineering Embryonic Stem-Cell Aggregation Allows an Enhanced Osteogenic Differentiation In Vitro. Tissue Eng Part C-Me. 2010;16:583-95.

[33] Huang B, Wu HK, Kim S, Zare RN. Coating of poly(dimethylsiloxane) with n-dodecyl-beta-D-maltoside to minimize nonspecific protein adsorption. Lab Chip. 2005;5:1005-7.

[34] Malda J, van Blitterswijk CA, van Geffen M, Martens DE, Tramper J, Riesle J. Low oxygen tension stimulates the redifferentiation of dedifferentiated adult human nasal chondrocytes. Osteoarthr Cartilage. 2004;12:306-13.

[35] Weiss HE, Roberts SJ, Schrooten J, Luyten FP. A Semi-Autonomous Model of Endochondral Ossification for Developmental Tissue Engineering. Tissue Eng Part A. 2012.

[36] Tekin H, Anaya M, Brigham MD, Nauman C, Langer R, Khademhosseini A. Stimuli-responsive microwells for formation and retrieval of cell aggregates. Lab Chip. 2010;10:2411-8.

[37] Witters D, Vergauwe N, Vermeir S, Ceyssens F, Liekens S, Puers R, et al. Biofunctionalization of electrowetting-on-dielectric digital microfluidic chips for miniaturized cell-based applications. Lab Chip. 2011;11:2790-4.

[38] Wu J, Wheeldon I, Guo Y, Lu T, Du Y, Wang B, et al. A sandwiched microarray platform for benchtop cell-based high throughput screening. Biomaterials. 2011;32:841-8.

[39] Demas JN, DeGraff BA, Coleman PB. Oxygen sensors based on luminescence quenching. Anal Chem. 1999;71:793a-800a.

[40] Wilkinson F, Abdel-Shafi AA. Mechanism of quenching of triplet states by molecular oxygen: Biphenyl derivatives in different solvents. J Phys Chem A. 1999;103:5425-35.

[41] De Bank PA, Hou QP, Warner RM, Wood IV, Ali BE, MacNeil S, et al. Accelerated formation of multicellular 3-D structures by cell-to-cell cross-linking. Biotechnol Bioeng. 2007;97:1617-25.

[42] Place ES, Evans ND, Stevens MM. Complexity in biomaterials for tissue engineering. Nat Mater. 2009;8:457-70.

[43] Chapman-Smith A, Cronan JE. In vivo enzymatic protein biotinylation. Biomol Eng. 1999;16:119-25.

[44] Tannous BA, Grimm J, Perry KF, Chen JW, Weissleder R, Breakefield XO. Metabolic biotinylation of cell surface receptors for in vivo imaging. Nat Methods. 2006;3:391-6.

[45] Zeng Y, Ramya TNC, Dirksen A, Dawson PE, Paulson JC. High-efficiency labeling of sialylated glycoproteins on living cells. Nat Methods. 2009;6:207-9.

[46] Howarth M, Chivers CE, Crozat E, Chu C, Moy VT, Sherratt DJ. A streptavidin variant with slower biotin dissociation and increased mechanostability. Nat Methods. 2010;7:391-U76.
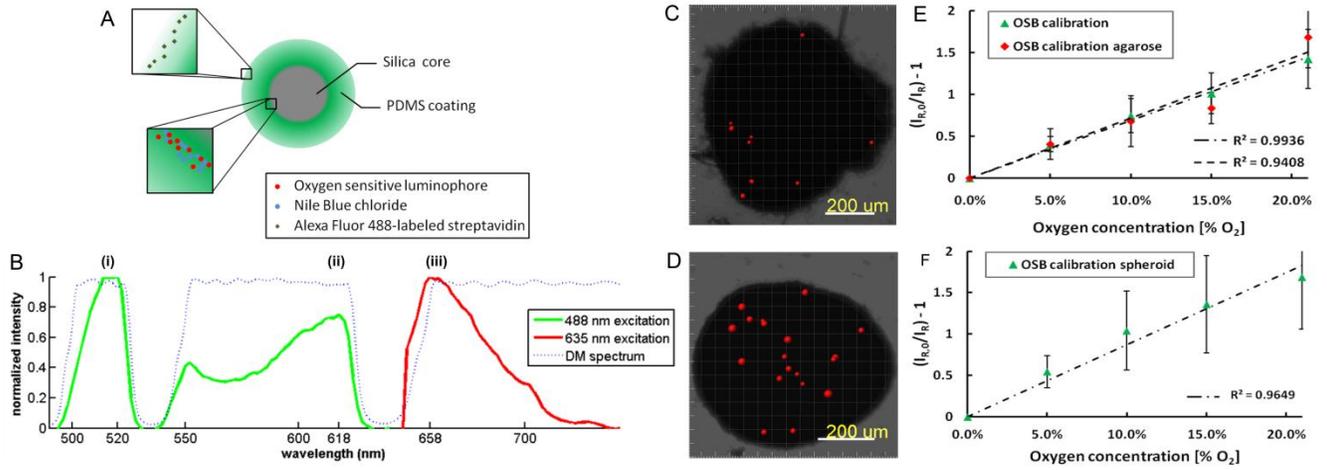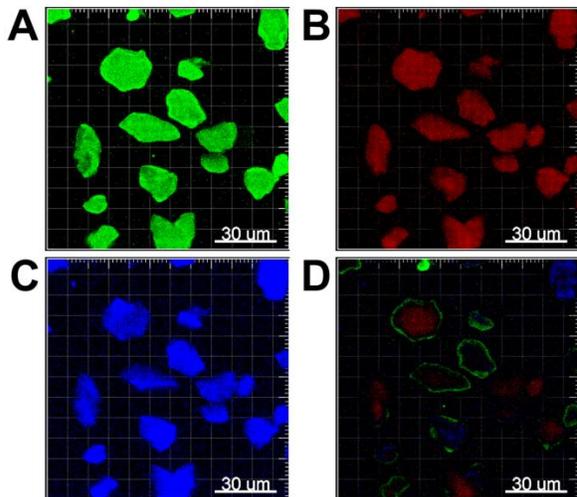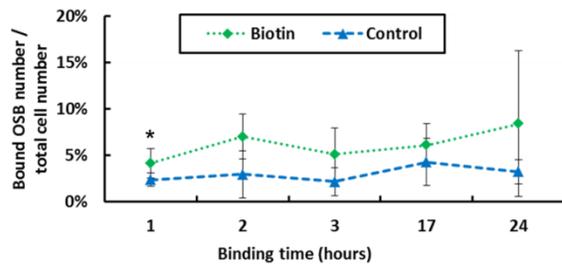
Figures

Figure 1

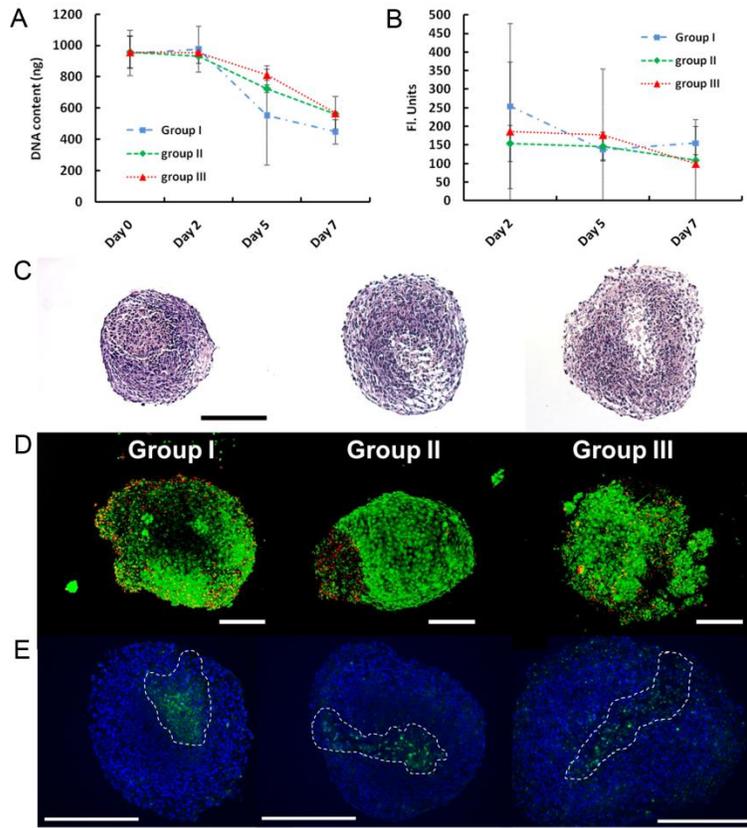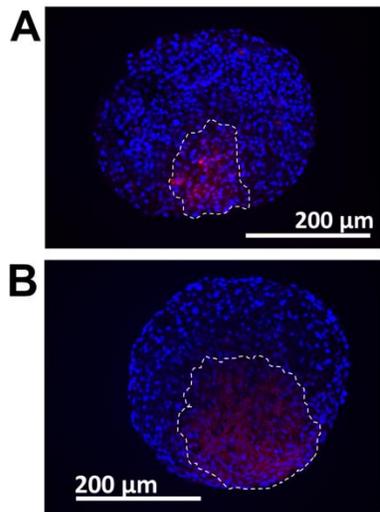**Figure 2**

Figure 3

Figure 4

Figure 5

Figure Captions

Figure 1. Characterization and calibration of oxygen sensitive microbeads (OSBs). (**A**) Design of the OSBs functionalized with Alexa Fluor 488 labelled streptavidin molecules. (**B**) Microspectroscopy of OSB fluorescence spectrum, with fluorescent excitation at 488 nm (green) or 635 nm (red). Emission peaks originate from (**i**) Alexa Fluor 488, (**ii**) ruthenium complex, and (**iii**) Nile Blue signal. Characteristic transmission spectrum of the dichroic mirror (DM) used for microspectroscopy is indicated by the dotted lines. Distribution of OSBs in an ATDC5 aggregate (~Ø 300 μm) cultivated for 4 days (**C**) without biotinylation of the cells and (**D**) with biotinylation of the cells. Images were obtained after data processing in Imaris Bitplane (Zurich, Switzerland). (**E**) Calibration curve obtained for OSBs suspended in a liquid (green triangles, $R^2 = 0.9936$) or with the use of an agarose spacer (red squares, $R^2 = 0.9408$). (**F**) Calibration curve obtained for OSBs integrated in a cell aggregate which was cultivated for 7 days ($R^2 = 0.9717$). Cells were blocked from respiration with NaN_3 to avoid potential influence of oxygen consumption on calibration data.

Figure 2. Confocal image of microbeads indicating the presence of three different fluorescent dyes; Alexa Fluor 488 labeled streptavidin (green, (**A**)), $Ru(Ph_2phen_3)Cl_2$ (red, (**B**)), and Nile Blue chloride (blue, (**C**)). Images show maximum intensity projections (MIP) obtained from a z-stack image acquisition. (**D**) Equalized intensity overlay of all three fluorescent images.

Figure 3. Conjugation stability assay of OSBs on 2-dimensional confluent ATDC5 cell monolayers. Untreated or biotinylated cell monolayers were incubated with 5% OSBs (particle number / total cell number) and assessed on stable microbead interaction. Figure shows the amount of cell-conjugated OSBs (particle number / total cell number) quantified at defined time points. (*) $p < 0.05$

Figure 4. The non-interfering incorporation of OSBs into ATDC5 aggregates was quantified over a 1 week cultivation period by assessment of (**A**) total DNA amount per aggregate, (**B**) cell metabolic activity, (**C**) aggregate morphology after 7 days of cultivation (Hematoxylin & Eosin staining) and (**D,E**) viability of seeded cells. This last aspect was quantified through both LIVE/DEAD viability assays (Invitrogen, live cells are green and dead cells are red) and TUNEL staining for determination of apoptotic cells (green colour indicates apoptotic cells and blue colour indicates the cell nuclei (DAPI counterstaining)). (Group I) no OSBs and no SB treatment, (Group II) SB treated cells, and (Group III) SB treated cells with OSB addition. Scalebars = 200 μm.

Figure 5. Pimonidazole staining of cell aggregates indicating hypoxic regions ($< 1\%\ O_2$). Aggregates were obtained from (**A**, Group I) untreated cells or (**B**, Group III) biotinylated cells with 0.2% OSB integration 7

days after initial aggregation (red regions indicate positive pimonidazole staining and blue color indicates the cell nuclei (DAPI)).
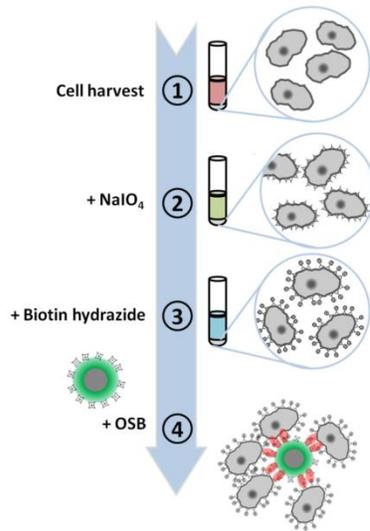
Supplementary Data

Figures

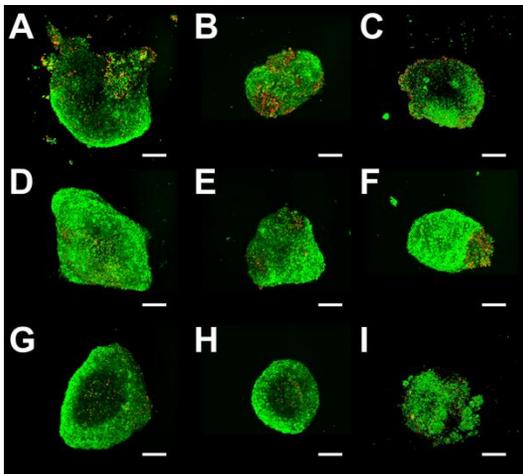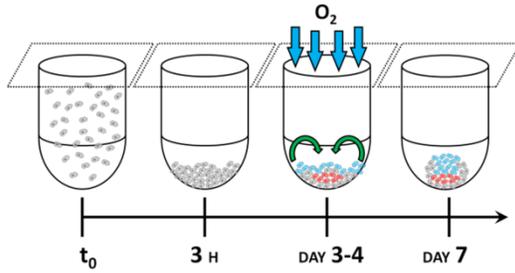
Figure S1

Figure S2

Figure S3

Supplementary Figure Captions

Figure S1. Schematic overview of OSB integration and aggregate formation process. (**1**) ATDC5 cells are harvested and (**2**) treated with sodium periodate to induce aldehyde groups at the cellular surfaces. (**3**) These aldehyde groups covalently bind biotin hydrazide which gives rise to biotinylated cell surfaces. (**4**) Biotinylated cells are transferred to medium containing streptavidin coated microbeads. Normal aggregation occurs with stable and efficient integration of the OSBs.

Figure S2. LIVE/DEAD viability images of ATDC5 aggregates. (**A-C**) Aggregates are obtained from untreated cells, (**D-F**) from biotinylated cells, or (**G-I**) from biotinylated cells integrated with 0.2% OSBs. Images were taken (**A,D,G**) after 2 days, (**B,E,H**) 5 days, or (**C,F,I**) 7 days of initial aggregation. Scalebars = 200 μm.

Figure S3. Illustration showing the fusing of aggregate edges after initial aggregation. Cells exposed to high oxygen tensions (blue cells) consume more oxygen than cells exposed to lower oxygen tensions (red cells), resulting from a Michaelis-Menten relationship for oxygen uptake. After an initial aggregation phase the cells with high oxygen uptake rate will become embedded into deeper regions of the aggregate, possibly resulting in the formation of hypoxic zones as observed in **Figure 5**.